

Magnetic field enhanced single particle tunneling in MoS_2-superconductor vertical Josephson junction

Wen-Zheng Xu(徐文正), Lai-Xiang Qin(秦来香), Xing-Guo Ye(叶兴国), Fang Lin(林芳), Da-Peng Yu(俞大鹏), Zhi-Min Liao(廖志敏)

Citation: Chin. Phys. B . 2020, 29(5): 057502 . **doi:** 10.1088/1674-1056/ab8209
Journal homepage: http://cpb.iphy.ac.cn; http://iopscience.iop.org/cpb

What follows is a list of articles you may be interested in

Nanofabrication of 50 nm zone plates through e-beam lithography with local proximity effect correction for x-ray imaging

Jingyuan Zhu(朱静远), Sichao Zhang(张思超), Shanshan Xie(谢珊珊), Chen Xu(徐晨), Lijuan Zhang(张丽娟), Xulei Tao(陶旭磊), Yuqi Ren(任玉琦), Yudan Wang(王玉丹), Biao Deng(邓彪), Renzhong Tai(邰仁忠), Yifang Chen(陈宜方)
Chin. Phys. B . 2020, 29(4): 047501 . **doi:** 10.1088/1674-1056/ab7800

Electrical transport and optical properties of Cd_3As_2 thin films

Yun-Kun Yang(杨运坤), Fa-Xian Xiu(修发贤), Feng-Qiu Wang(王枫秋), Jun Wang(王军), Yi Shi(施毅)
Chin. Phys. B . 2019, 28(10): 107502 . **doi:** 10.1088/1674-1056/ab3a91

Magnetoresistance hysteresis in topological Kondo insulator SmB_6 nanowire

Ling-Jian Kong(孔令剑), Yong Zhou(周勇), Hua-Ding Song(宋化鼎), Da-Peng Yu(俞大鹏), Zhi-Min Liao(廖志敏)
Chin. Phys. B . 2019, 28(10): 107501 . **doi:** 10.1088/1674-1056/ab3a89

Two-dimensional transport and strong spin-orbit interaction in $SrMnSb_2$

Jiwei Ling(凌霁玮), Yanwen Liu(刘彦闻), Zhao Jin(金昭), Sha Huang(黄沙), Weiyi Wang(王伟懿), Cheng Zhang(张成), Xiang Yuan(袁翔), Shanshan Liu(刘姗姗), Enze Zhang(张恩泽), Ce Huang(黄策), Raman Sankar, Fang-Cheng Chou, Zhengcai Xia(夏正才), Faxian Xiu(修发贤)
Chin. Phys. B . 2018, 27(1): 017504 . **doi:** 10.1088/1674-1056/27/1/017504

Total ionizing radiation-induced read bit-errors in toggle magnetoresistive random-access memory devices

Yan Cui(崔岩), Ling Yang(杨玲), Teng Gao(高腾), Bo Li(李博), Jia-Jun Luo(罗家俊)
Chin. Phys. B . 2017, 26(8): 087501 . **doi:** 10.1088/1674-1056/26/8/087501

SPECIAL TOPIC — Topological 2D materials

Magnetic field enhanced single particle tunneling in MoS_2–superconductor vertical Josephson junction*

Wen-Zheng Xu(徐文正)[1], Lai-Xiang Qin(秦来香)[1], Xing-Guo Ye(叶兴国)[1], Fang Lin(林芳)[1], Da-Peng Yu(俞大鹏)[2], and Zhi-Min Liao(廖志敏)[1,3,†]

[1] *State Key Laboratory for Mesoscopic Physics and Collaborative Innovation Center of Quantum Matter, School of Physics, Peking University, Beijing* 100871, *China*

[2] *Shenzhen Institute for Quantum Science and Engineering and Department of Physics, Southern University of Science and Technology, Shenzhen* 518055, *China*

[3] *Frontiers Science Center for Nano-optoelectronics, Peking University, Beijing* 100871, *China*

(Received 14 January 2020; revised manuscript received 11 February 2020; accepted manuscript online 23 March 2020)

As a prototypical transition-metal dichalcogenide semiconductor, MoS_2 possesses strong spin–orbit coupling, which provides an ideal platform for the realization of interesting physical phenomena. Here, we report the magnetotransport properties in NbN–MoS_2–NbN sandwich junctions at low temperatures. Above the critical temperature around ∼11 K, the junction resistance shows weak temperature dependence, indicating a tunneling behavior. While below ∼11 K, nearly zero junction resistance is observed, indicating the superconducting state in the MoS_2 layer induced by the superconducting proximity effect. When a perpendicular magnetic field ∼1 T is applied, such proximity effect is suppressed, accompanying with insulator-like temperature-dependence of the junction resistance. Intriguingly, when further increasing the magnetic field, the junction conductance is significantly enhanced, which is related to the enhanced single particle tunneling induced by the decrease of the superconducting energy gap with increasing magnetic fields. In addition, the possible Majorana zero mode on the surface of MoS_2 can further lead to the enhancement of the junction conductance.

Keywords: proximity effect, transition metal dichalcogenides, magnetotransport

PACS: 74.45.+c, 75.47.–m, 73.43.Qt **DOI:** 10.1088/1674-1056/ab8209

Layered transition metal dichalcogenides (TMDs) have attracted much attention recently because of their rich physical properties.[1–11] As a typical TMD, MoS_2 possesses a direct band gap around ∼ 1.8–1.9 eV in its single layer, in contrast to the indirect band gap in its multilayer counterpart.[9] Gate-induced superconductivity[5–9] can occur in MoS_2. Due to the presence of spin–orbit coupling (SOC),[2,9] an effective Zeeman field will be formed in MoS_2. When the effective Zeeman field locks the Cooper pairs in the direction orthogonal to the in-plane magnetic field, the Zeeman effect can protect the superconductivity, thus greatly improving the in-plane critical field B_{C2}, which is the characteristic of Ising superconductor.[10,11] In addition, the superconductivity of MoS_2 can also be achieved through the proximity effect. The interlayer of MoS_2 is bound by van der Waals force, so the few layers of MoS_2 can be easily obtained through the mechanical exfoliation method.[12] And the surface of MoS_2 is very flat,[12] promising the fine interface contact of the heterojunction, which provides an ideal platform for future application. Importantly, MoS_2 possesses strong SOC,[2] in contrast to the small SOC in graphene, which makes MoS_2 a promising candidate for spintronic effects. It is also predicted that the topological superconducting phase and the Majorana zero mode[13–15] could emerge in the MoS_2–superconductor hybrid structures.[16,17] The singular non-Abelian exchange properties of Majorana zero modes would lead to the progress of quantum computation.[18–20]

Here, NbN is used to induce the superconductivity of MoS_2. As a type-II superconductor, NbN has a high critical temperature (∼ 15 K)[21–23] and a large upper critical magnetic field (∼ 25 T).[21] Its ultra-high critical magnetic field allows us to study the interface effect under a strong magnetic field.

In this study, we have fabricated an NbN–MoS_2–NbN vertical junction and investigated its low temperature magnetotransport properties. Without applying the magnetic field, the NbN electrode can well induce the MoS_2 nanosheet to the superconducting state below the critical temperature ∼ 11 K. Distinguish from the nearly zero resistance in the superconductivity state, an insulator-like behavior rises when a magnetic field ∼ 1 T is applied. Due to the magnetic field, the superconducting proximity effect is weakened, and the superconductivity behavior is absent. In the thermal activation region, the resistance increases exponentially following the Ar-

*Project supported by the National Key Research and Development Program of China (Grant Nos. 2018YFA0703703 and 2016YFA0300802) and the National Natural Science Foundation of China (Grant Nos. 91964201, 61825401, and 11774004).

†Corresponding author. E-mail: liaozm@pku.edu.cn

© 2020 Chinese Physical Society and IOP Publishing Ltd

rhenius formula. Below the temperature around ∼ 4 K, due to the enhancement of the proximity effect at low temperatures and multiple Andreev reflection, the trend of resistance rise is slowed down. Importantly, when further increasing the magnetic fields, a significant decrease of the junction resistance is obtained. Such reduction of the resistance is attributed to the tunneling current of single particle enhanced by magnetic field. Besides, the possible Majorana zero mode on the surface of MoS_2 may also make contribution to the reduction of the junction resistance.

MoS_2 nanosheets were obtained from bulk MoS_2 crystals by mechanical peeling method with thickness around ∼ 3 nm. Using electron beam lithography, NbN bottom electrodes were deposited on a 280 nm thick SiO_2/Si substrate by magnetron sputtering. Then, the prepared MoS_2 sheets were transferred to the NbN bottom electrode by dry transfer[24] technology, and finally the NbN top electrode was prepared to form a sandwich structure. The schematic diagram of the NbN–MoS_2–NbN vertical junction device is shown in Fig. 1(a). The optical image and measurement schematic diagram of the NbN–MoS_2–NbN superconducting vertical junction are shown in Fig. 1(b). The transporting properties of the vertical junction were characterized by the crossbar measurement, in which the current source was applied between terminal 1 and terminal 4, and the voltage was measured between terminal 2 and terminal 3. The constant current applied in this experiment is 0.1 μA. The direction of the applied magnetic field is perpendicular to the junction surface and parallel to the current.

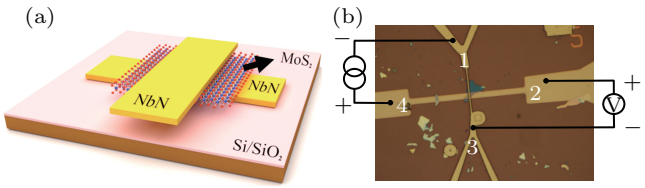


Fig. 1. (a) The schematic diagram of the NbN–MoS_2–NbN vertical junction device. From bottom to top, the order is SiO_2/Si substrate, NbN bottom electrode, MoS_2 nanosheet, and NbN top electrode. (b) An optical image of the NbN–MoS_2–NbN vertical junction. Terminal 2 and terminal 4 are bottom electrodes. Terminal 1 and terminal 3 are top electrodes.

Figure 2 (a) shows the vertical junction resistance as a function of temperature under different magnetic fields. Before the NbN electrodes enter the superconducting state, the magnetic field has no effect on the junction resistance. In contrast, the R–T curves begin to diverge under different magnetic fields (0–7 T) below the critical temperatures. When there is no magnetic field, the resistance decreases to almost zero at low temperature, indicating the superconductivity of MoS_2 caused by the superconducting proximity effect.[25,26] However, when an external magnetic field ∼ 1 T is applied, the superconducting proximity effect is suppressed and nearly zero resistance disappears. With the decrease of temperature, the vertical junction resistance first decreases and then increases, showing an insulator-like behavior. The magnetic field can penetrate the NbN electrodes through the vortex structure,[21–23] thus localizing the superconducting proximity effect on the surface of MoS_2, making the MoS_2 flake a superconducting–normal state–superconducting structure. Intriguingly, when further increasing the magnetic fields, despite a similar insulator-like behavior also emerges, the resistance is significantly reduced.

The relationship between the NbN electrode transition temperatures and the magnetic field is analyzed. There exist two steep decreases in the resistance between 9 K and 14 K, as shown in the inset of Fig. 2(a), indicating the different transition temperatures of the top and bottom electrodes. When the resistance is 90% of the normal state resistance, the corresponding temperature is defined as the transition temperature. The transition temperatures of the two electrodes are denoted as T_{C1} and T_{C2}, respectively. The magnetic field dependence of T_{C1} and T_{C2} is shown in Fig. 2(b). With the increase of the magnetic field, both T_{C1} and T_{C2} decrease gradually.

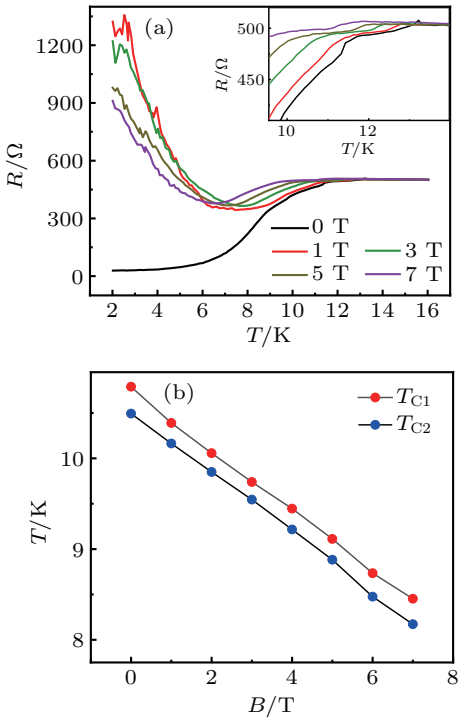


Fig. 2. (a) Temperature dependence of the vertical junction resistance under different magnetic fields. The inset is the zoom-in view of (a). The junction resistance shows two steep decreases between 9 K and 14 K, as shown in the inset, which correspond to the beginning of superconducting state at the two NbN electrodes, respectively. (b) Magnetic field dependence of T_{C1} and T_{C2}. The transition temperature is defined as the temperature corresponding to the reduction of resistance to 90% of the normal state.

The insulator-like behavior under different magnetic fields [Fig. 2(a)] is analyzed in detail. In the thermal activation region, the junction resistance can be described by the formula $R \propto e^{\Delta_b/k_B T}$, where k_B is the Boltzmann constant and Δ_b is the transport barrier height[27,28] (a Schottky barrier). As the temperature decreases, the number of thermally activated

electrons decreases, which leads to an exponential increase in resistance. Figure 3 (a) shows the Arrhenius plots $\ln R$–$1/T$ under different magnetic fields. The barrier heights under different magnetic fields are calculated according to the slopes of the red dotted lines, as shown in Fig. 3(b). When the temperature is around 4–6 K, the behavior of thermally activated electrons dominates the junction resistance. With the increase of the magnetic field, the barrier height decreases from 0.75 meV at 1 T to 0.38 meV at 7 T. The relationship between $\ln R$ and $1/T$ deviates from the linear dependence at 2–4 K. This is due to the following reasons: (i) the superconducting proximity effect is further strengthened at low temperatures, and thus the thickness of MoS_2 that is not transformed into superconductivity state is further thinned; (ii) at low temperatures, the multiple Andreev reflection[29] is also enhanced, which can also make contribution to the reduction of the junction resistance.

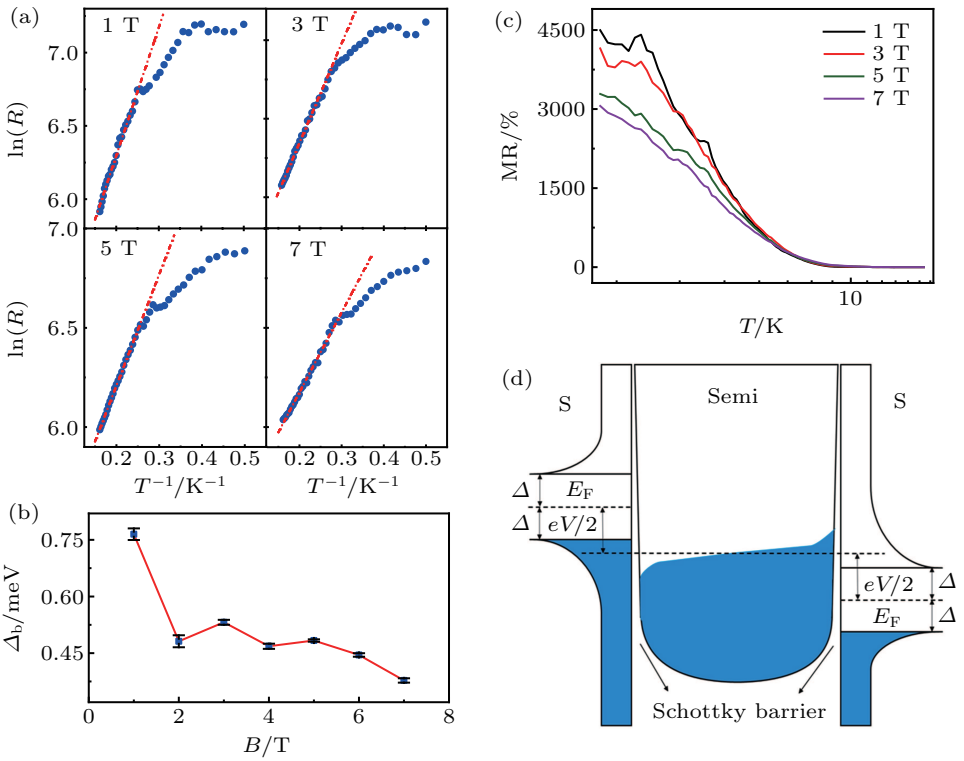


Fig. 3. (a) The Arrhenius plots of the junction resistance at 2–6 K under different magnetic fields. The barrier height Δ_b can be obtained by fitting the linear region. (b) The magnetic field dependence of the barrier height. The error bar is estimated from the standard deviation of the linear fitting. (c) Magnetoresistance (MR) as a function of temperature under different magnetic fields of 1–7 T. The MR is defined as MR $= \frac{R(B)-R(B=0\ \mathrm{T})}{R(B=0\ \mathrm{T})} \times 100\%$. Below the transition temperature, the magnetic field can obviously reduce the MR. (d) The energy diagram of superconductor–semiconductor–superconductor junction. "S" represents the superconducting NbN electrode layer and the superconducting MoS_2 layer, and "Semi" represents the normal MoS_2 flake.

In order to further analyze the effect of the magnetic field on the junction resistance, we studied the relationship between magnetoresistance (MR) and temperature under different magnetic fields as shown in Fig. 3(c). The MR is defined as MR $= \frac{R(B)-R(B=0\ \mathrm{T})}{R(B=0\ \mathrm{T})} \times 100\%$. Above the critical temperature of the NbN electrodes, the magnetic field has no effect on the MR. However, below around ~ 10 K, the MR increases with decreasing temperature. Intriguingly, a large magnetic field can significantly reduce the MR, for example, from about 4500% under 1 T to about 3000% under 7 T at 2 K. This phenomenon can be described by the single particle tunneling model.[30] Because the MoS_2 superconducting layer induced by the proximity effect is very thin relative to the NbN electrode, the change of the energy gap near the interface can be neglected. So the whole vertical junction is an S–Semi–S structure, in which "S" represents the superconducting NbN electrode layer and the superconducting MoS_2 layer, and "Semi" represents the normal MoS_2 flake [Fig. 3(d)]. When a superconductor contacts with a semiconductor, a Schottky barrier[31] will be formed at the contact position, so the S–Semi–S junction can be equivalent to two superconducting–insulator–normal state (SIN) junctions in series,[32] i.e., an SINIS junction. For an SIN junction, its tunneling current can be described as[33]

$$I(V) = \frac{1}{eG_{\mathrm{T}}} \int_{-\infty}^{+\infty} N(E)\,[f(E-eV) - f(E)]\,\mathrm{d}E,$$

where $f(E)$ is the Fermi distribution function, V is the voltage through the junction, e is the elementary charge, and G_{T} is the tunneling conductance related to the thickness of MoS_2 which has not been transformed into superconducting state. The density of states (DOS) of the NbN electrodes is described by the

Dynes model[34]

$$N(E) = \left| \mathrm{Re}\left[\frac{E - \mathrm{i}\Gamma}{\sqrt{(E - \mathrm{i}\Gamma)^2 - \Delta^2}} \right] \right|,$$

where Γ is the Dynes parameter, and Δ is the superconducting energy gap that varies with the temperature and magnetic field. The superconducting gap decreases with the increase of the magnetic field, which will lead to the increase of the number of thermally activated electrons participating in conduction and thus reduce the junction resistance.

Besides, Majorana zero modes are predicted to exist in semiconductor–superconductor heterostructures.[17] Recently, a quantized zero-bias peak has been found in indium antimonide semiconductor–superconductor hybrid device,[13] which is regarded as signatures of Majorana fermions. Moreover, it is also proposed that Majorana zero modes could emerge in semiconductor with strong SOC coupled to an s-wave superconductor and a ferromagnetic insulator.[17] In this work, the NbN electrodes could induce MoS_2 into superconductivity through proximity effect. Due to the strong SOC of MoS_2,[35] the effective Zeeman fields could polarize the electron spins to the out-of-plane directions and induce an effective Zeeman gap. When an external magnetic field is applied, the topological superconducting phase could emerge on the interface of NbN and MoS_2. Majorana zero modes may appear on the surface of MoS_2, and it will participate in the tunneling process, thus further reducing the resistance of the vertical junction. However, the direct detection of Majorana fermions in such systems needs further theoretical and experimental investigations.

In summary, we have prepared an NbN–MoS_2–NbN vertical superconducting junction and analyzed its low temperature transport properties under different magnetic fields. Above the critical temperature ~ 11 K, the junction resistance shows weak response to the temperature. Below ~ 11 K, the superconducting behavior emerges due to the proximity effect. However, when a magnetic field ~ 1 T is applied, the proximity effect is suppressed and the insulator-like temperature dependence of the junction resistance is observed. Within the thermal activation regime, the resistance follows the Arrhenius formula, while a deviation is obtained below ~ 4 K. With the increase of the magnetic fields, both the critical temperatures and the barrier heights decrease. Importantly, at low temperatures, the vertical junction resistance shows significant reduction when increasing the magnetic field above 1 T, which is attributed to the enhanced single particle tunneling current induced by the decrease of the superconducting energy gap. In addition, the possible Majorana zero mode will further contribute to the reduction of the junction resistance.

References

[1] Zeng S M, Zhao Y C, Li G and Ni J 2016 *Phys. Rev. B* **94** 024501
[2] Klinovaja J and Loss D 2013 *Phys. Rev. B* **88** 075404
[3] Roldán R, Cappelluti E and Guinea F 2013 *Phys. Rev. B* **88** 054515
[4] Zhang R Y, Tsai I L , Chapman J, Khestanova E, Waters J and Grigorieva I V 2016 *Nano Lett.* **16** 629
[5] Costanzo D, Jo S, Berger H and Morpurgo A F 2016 *Nat. Nanotechnol.* **11** 339
[6] Taniguchi K, Matsumoto A, Shimotani H and Takagi H 2012 *Appl. Phys. Lett.* **101** 042603
[7] Saito Y, Nakamura Y, Bahramy M S, Kohama Y, Ye J T, Kasahara Y, Nakagawa Y, Onga M, Tokunaga M, Nojima T, Yanase Y and Iwasa Y 2016 *Nat. Phys.* **12** 144
[8] Ye J T, Zhang Y J, Akashi R, Bahramy M S, Arita R and Iwasa Y 2012 *Science* **338** 1193
[9] Yuan N F Q, Mak K F and Law K T 2014 *Phys. Rev. Lett.* **113** 097001
[10] Lu J M, Zheliuk O, Leermakers I, Yuan N F Q, Zeitler U, Law K T and Ye J T 2015 *Science* **350** 1353
[11] Zhou B T, Yuan N F Q, Jiang H L and Law K T 2016 *Phys. Rev. B* **93** 1850501(R)
[12] Ganatra R and Zhang Q 2014 *ACS Nano* **8** 4074
[13] Zhang H, Liu C X, Gazibegovic S, Xu D, Logan J A, Wang G, Loo N, Bommer J D S, Moor M W A, Car D, Op het Veld R L M, Veldhoven P J, Koelling S, Verheijen M A, Pendharkar M, Pennachio D J, Shojaei B, Lee J S, Palmstrøm C J, Bakkers E P A M, Sarma S D and Kouwenhoven L P 2018 *Nature* **556** 74
[14] Jose P S, Prada E and Aguado R 2014 *Phys. Rev. Lett.* **112** 137001
[15] Gül Ö Zhang H, Bommer J D S, Moor M W A, Car D, Plissard S R, Bakkers E P A M, Geresdi A, Watanabe K, Taniguchi T and Kouwenhoven L P 2018 *Nat. Nanotechnol* **13** 192
[16] Lin C H, Sau J D and Sarma S D 2012 *Phys. Rev. B* **86** 224511
[17] Alicea J 2010 *Phys. Rev. B* **81** 125318
[18] Kitaev A Y 2003 *Ann. Phys.* **303** 2
[19] Halperin B I, Oreg Y, Stern A, Refael G, Alicea J and von Oppen F 2012 *Phys. Rev. B* **85** 144501
[20] Elliott S R and Franz M 2015 *Rev. Mod. Phys.* **87** 137
[21] Mathur M P, Deis D W and Gavaler J R 1972 *J. Appl. Phys.* **43** 3158
[22] Beck M, Klammer M, Lang S, Leiderer P, Kabanov V V, Gol'tsman G N and Demsar J 2011 *Phys. Rev. Lett.* **107** 177007
[23] Noat Y, Cherkez V, Brun C, Cren T, Carbillet C, Debontridder F, Ilin K, Siegel M, Semenov A, Hübers H W and Roditchev D 2013 *Phys. Rev. B* **88** 014503
[24] Georgiou T, Jalil R, Belle B D, Britnell L, Gorbachev R V, Morozov S V, Kim Y J, Gholinia A, Haigh S J, Makarovsky O, Eaves L, Ponomarenko L A, Geim A K, Novoselov K S and Mishchenko A 2013 *Nat. Nanotechnol.* **8** 100
[25] Takayanagi H and Kawakami T 1985 *Phys. Rev. Lett.* **54** 2449
[26] McMillan W L 1968 *Phys. Rev.* **175** 537
[27] Zhang L, Yan Y, Wu H C, Yu D P, Liao Z M 2016 *ACS Nano.* **10** 3816
[28] Britnell L, Gorbachev R V, Jalil R, Belle B D, Schedin F, Mishchenko A, Georgiou T, Katsnelson M I, Eaves L, Morozov S V, Peres N M R, Leist J, Geim A K, Novoselov K S and Ponomarenko L A 2012 *Science* **335** 947
[29] Kleinsasser A W, Miller R E, Mallison W H and Arnold G B 1994 *Phys. Rev. Lett.* **72** 1738
[30] Blonder G E, Tinkham M and lapwijk T M K 1982 *Phys. Rev. B* **25** 4515
[31] Tkachov G and Fal'ko V I 2004 *Phys. Rev. B* **69** 092503
[32] Kleinsasser A W and Kastalsky A 1993 *Phys. Rev. B.* **47** 8361
[33] Koppinen P J, Kühn T and Maasilta I J 2009 *J. Low Temp. Phys.* **154** 179
[34] Dynes R C, Narayanamurti V and Garno J P 1978 *Phys. Rev. Lett.* **41** 1509
[35] MolinaS ánchez A, Sangalli D, Hummer K, Marini A and Wirtz L 2013 *Phys. Rev. B* **88** 045412